The Canadian Mineralogist
Vol. 44, pp. 1387-1402 (2006)

NATURAL RADIATION-INDUCED DAMAGE IN QUARTZ. II. DISTRIBUTION AND IMPLICATIONS FOR URANIUM MINERALIZATION IN THE ATHABASCA BASIN, SASKATCHEWAN, CANADA

SANDA BOTIS, YUANMING PAN[§], THOMAS BONLI, YINGKAI XU, AIMIN ZHANG AND SERGIY NOKHRIN

Department of Geological Sciences, University of Saskatchewan, Saskatoon, Saskatchewan S7N 5E2, Canada

VLAD SOPUCK

Cameco Corporation, 2121 11th Street West, Saskatoon, Saskatchewan S7M 1J3, Canada

ABSTRACT

The distribution of natural radiation-induced damage in quartz from the uranium-mineralized Athabasca basin in northern Saskatchewan has been investigated by cathodoluminescence (CL) imaging and electron paramagnetic resonance (EPR) spectroscopy. With CL imaging, it is not only possible to distinguish two generations of overgrowths on detrital quartz, but also to reveal three types of alpha-particle-induced damage in quartz: 1) halos around inclusions of U- and Th-bearing minerals, 2) patches in contact with U-bearing minerals in matrices or pores, and 3) continuous rims in samples with or without any U-bearing minerals. CL halos in detrital quartz grains are mostly associated with zircon inclusions, whereas those in overgrowths mainly surround crandallite inclusions. CL patches are widespread, but are particularly abundant in altered sandstones close to the sandstone–basement unconformity and faults. Continuous CL rims occur not only in mineralized rocks close to the unconformity at the Key Lake deposit, but are pervasively developed in the siliceous cap and along the unconformity at the McArthur River deposit and the neighboring BJ prospect. With EPR, which is more sensitive in detecting dilute radiation-induced defects than CL, we confirm the results of CL imaging that radiation-induced defects are best developed in quartz grains from the unconformity, lithological boundaries, faults and fractures. Continuous CL rims on quartz grains most likely formed from bombardments of alpha particles emitted from U-bearing fluids. The restricted occurrences of continuous CL rims suggest channelized uranium-bearing fluids in the Athabasca basin. The presence of continuous CL rims on detrital quartz grains and the local abundance of U-bearing minerals in both generations of overgrowths suggest that uranium was present in early diagenetic fluids and that mineralization commenced during the early stage of diagenesis and continued during the peak diagenesis. The absence of radiation-induced damage in quartz from altered basement rocks below the McArthur River deposit supports our proposal that basement fluids were poor in uranium. The common occurrence of radiation-induced damage in quartz from reactivated fractures, faults and voids provides further evidence for late remobilization of uranium.

Keywords: radiation-induced damage, quartz, cathodoluminescence, electron paragmagnetic resonance, uranium mineralization, Athabasca basin, Saskatchewan.

SOMMAIRE

Nous évaluons la distribution du dommage dû à la radiation dans le quartz provenant des zones minéralisées en uranium dans le bassin d'Athabasca, dans le nord du Saskatchewan, selon des images de la distibution de la cathodoluminescence (CL) et la spectroscopie de la résonance paramagnétique des électrons (EPR). Dans les images CL, il est non seulement possible de distinguer deux générations de surcroissances sur le quartz détritique, mais aussi de reconnaître trois sortes de dommage dû au particules alpha: 1) aureoles autour des inclusions de minéraux uranifères et thorifères, 2) taches dans le quartz près des minéraux uranifères dans la matrice ou les pores, et 3) liserés continus dans les grains avec ou sans minéraux uranifères. Les aureoles CL dans les grains de quartz détritique apparaissent surtout autour des grains de zircon inclus, tandis que celles dans les surcroissances seraient surtout dues aux inclusions de crandallite. Les taches de CL sont répandues, mais apparaissent surtout dans les grès altérés près du contact discordant avec le socle ou près de failles. Les liserés cathodoluminescents continus se trouvent non seulement dans les roches minéralisées près de la discordance au gisement de Key Lake, mais ils sont aussi répandus dans la coiffe siliceuse et le long de la discordance au gisement de McArthur River et à l'indice BJ, avoisinant. Avec la méthode EPR, qui est plus sensible que CL pour détecter le dommage dû à des défauts à un niveau plus faible, nous pouvons confirmer les résultats des images CL, que les défauts dus à la radiation sont le plus évidents dans les grains de quartz près de la discordance et des contacts lithologiques, failles et fractures. Les liserés cathodoluminescents continus sur les grains de quartz résulteraient probablement de bombardements de particules alpha émises à partir des fluides uranifères. D'après la distribution limitée de

§ *E-mail address*: yuanming.pan@usask.ca

ces liserés, nous entrevoyons une circulation canalisée des fluides uranifères. La présence de tels liserés sur les grains de quartz détritiques et l'abondance locale des minéraux porteurs d'uranium dans les deux générations de surcroissance font penser que l'uranium était présent dans la phase fluide responsable de la diagenèse et que la minéralisation a commencé avec la diagenèse et a continué jusqu'à son apogée. D'après l'absence des témoins du dommage dû à la radiation dans le quartz provenant des rocles du socle au dessous du gisement de McArthur River, les fluides circulant dans le socle étaient pauvres en uranium. La présence d'endommagement dans le quartz provenant de fractures et failles réactivées et dans les cavités démontre la remobilisation tardive de l'uranium.

(Traduit par la Rédaction)

Mots-clés: dommage dû à la radiation, quartz, cathodoluminescence, résonance paragmagnétique des électrons, minéralisation en uranium, bassin d'Athabasca, Saskatchewan.

Introduction

The Paleoproterozoic Athabasca basin in northern Saskatchewan (Fig. 1) is the site of several large, high-grade unconformity-type uranium deposits (*e.g.*, the McArthur River deposit containing an average grade of 20 wt% U_3O_8, and locally up to 70 wt% U_3O_8). These deposits collectively represent approximately 20% of the world's production of this economically and strategically important material. Quartz grains from the Athabasca basin, especially those in mineralized samples, have experienced large doses of alpha particle bombardments (as well as beta particles and gamma rays) and are expected to exhibit abundant natural radiation-induced damage. As part of our ongoing effort to study damage in minerals and other materials due to natural radiation, we have investigated quartz grains from the Athabasca basin by use of cathodoluminescence (CL) imaging, CL spectroscopy, micro-Raman spectroscopy, and electron paramagnetic resonance (EPR) spectroscopy (Zhang *et al.* 2002, Botis *et al.* 2004, 2005). In part I of this study, we reported a detailed CL and EPR study of quartz grains from one representative sample of mineralized sandstones (*i.e.*, H737–58 from the McArthur River deposit), which is characterized by pervasive development of radiation-damage-induced CL (Botis *et al.* 2005). Our EPR measurements and spectral simulations of isochronally annealed products of sample H737–58, particularly on the basis of differences in thermal properties and saturation behavior, allowed us to identify six paramagnetic centers {*i.e.*, one oxygen vacancy center (E_1'), three silicon vacancy-hole centers [O_2^{3-}/H^+(I), O_2^{3-}/H^+(II) and O_2^{3-}/M^+] and two O^{2-} peroxy radicals}. Moreover, EPR measurements of sample H737–58 after sequential HF-dissolution treatments showed that all paramagnetic centers except for E_1' are concentrated in the radiation-damaged rims and fractures. Also, correlations between CL spectra and

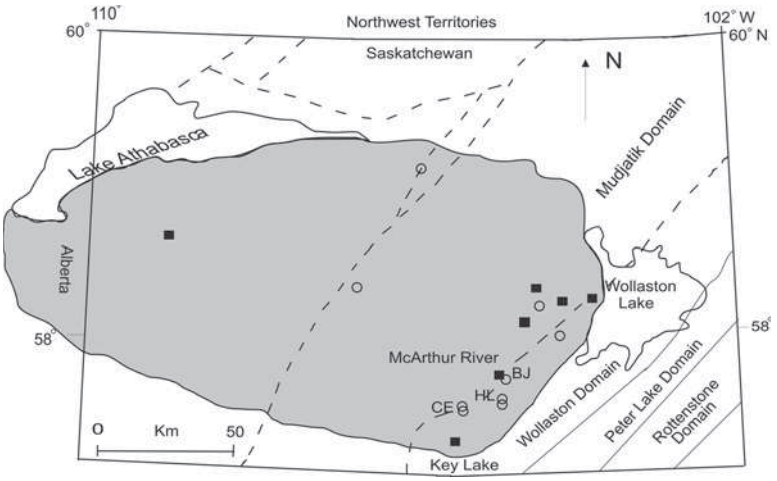

FIG. 1. Location map of the Athabasca basin, northern Saskatchewan. Sample locations in this study are marked by solid squares (uranium deposits) and open circles (exploration areas). Only those mentioned in the text are labeled: the Cigar Lake, Key Lake and McArthur River deposits, the BJ prospect, the Hughes Lake (HL) project, and the Cree Extension (CE) project.

paramagnetic centers from the isochronal annealing experiments suggested that the silicon vacancy centers are most likely responsible for an ultraviolet CL band at ~350 nm that is annealed out below 600°C, whereas the peroxy radicals correspond to a broad band of red CL at ~620–650 nm that persists at 600°C and above (Botis *et al*. 2005).

In this contribution, we provide detailed documentation of the development and distribution of natural radiation-induced damage in quartz grains from the Athabasca basin, particularly with respect to mineral paragenesis, stratigraphy and structure in two uranium deposits, the Key Lake and McArthur River deposits, and other selected locations in the eastern part of the Athabasca basin, by combined CL imaging and EPR spectroscopy. Several investigators have described well-developed radiation-damage-induced CL in quartz grains from sandstones, including CL rims on quartz in sandstones from uranium deposits (Morton 1978, Meunier *et al*. 1990, Komuro *et al*. 1995, Götze *et al*. 2001). We present evidence to suggest that CL rims on quartz grains from the Athabasca basin record bombardments of alpha particles emitted from U-bearing fluids. Also, the development and distribution of radiation-induced damage, as revealed by integrated CL imaging and EPR spectroscopy, place new constraints on the timing and sources of uranium mineralization in the Athabasca basin and are potentially useful in exploration for new uranium deposits in other sedimentary basins.

Geological Setting

The Paleoproterozoic Athabasca basin, consisting of redbed sandstones and conglomerates of the Athabasca Group, unconformably overlies a crystalline basement of Archean granitic gneisses and Paleoproterozoic metasedimentary rocks that have been metamorphosed to middle and upper amphibolite facies (Fig. 1, Armstrong & Ramaekers 1985).

The Athabasca Group consists of an approximately flat-lying, 2000 m sequence of mineralogically mature sandstones and conglomerates, interrupted by two marine intercalations, the Wolverine Point Formation at about 1000 m above the basin floor, and the Douglas and Carswell formations, consisting of organic-matter-rich shales and stromatolitic dolomites at the top of the sequence. The dominant lithological units of the Athabasca Group in the eastern Athabasca basin are those of the Manitou Falls Formation (Armstrong & Ramaekers 1985). The sandstones of the Manitou Falls Formation consist predominantly of detrital quartz grains, which are cemented by secondary quartz, hematite and clay minerals (dickite, kaolinite, chlorite and illite; Zhang *et al*. 2001). Accessory minerals include fluorapatite, zircon and tourmaline. Studies of the clay minerals and stratigraphy of the Athabasca basin, coupled with a microthermometric analysis of fluid inclusions in quartz overgrowths, indicate that the sandstones were buried to a maximum depth of 5–7 km and reached 200°C (Hoeve & Quirt 1984, Kyser *et al*. 2000).

Cumming & Krstic (1992) reported fluorapatite U–Pb ages of 1650–1700 Ma and interpreted them to represent the minimum age of deposition of the Athabasca Group. Kotzer *et al*. (1992) documented paleomagnetism in the Athabasca basin and suggested that the early diagenesis responsible for the formation of regional hematite had occurred at 1600–1750 Ma. Kotzer & Kyser (1995) obtained a Rb–Sr isochron age of 1477 ± 57 Ma for authigenic illite from an unaltered sandstone and interpreted it to represent the timing of peak diagenesis.

The uranium deposits in the Athabasca basin are commonly situated at the intersections of the sandstone–basement unconformity and late faults (Hoeve & Sibbald 1978, Hoeve & Quirt 1984, Percival *et al*. 1993, Kotzer & Kyser 1995, Fayek & Kyser 1997). Fayek & Kyser (1997) subdivided the uranium deposits in the Athabasca basin into two groups: 1) complex type and 2) simple type. The complex-type deposits are located at the unconformity, hosted partially by sandstones, and are characterized by the presence of abundant Ni–Co–As–Fe–Cu–Pb sulfides and arsenides. The simple-type deposits are situated entirely within faults and fractures in basement rocks and are characterized by a general lack of sulfides and arsenides. Fayek *et al*. (2002) reported U–Pb ages of 1486 to 1519 Ma for uraninite by secondary-ion mass spectrometry and interpreted them to represent the timing of primary mineralization in the Athabasca basin. A widely accepted model for the origin of the uranium deposits in the Athabasca basin is the hydrothermal-diagenetic model, initially proposed by Hoeve & Sibbald (1978) and further developed by Hoeve & Quirt (1984) and Fayek & Kyser (1997). In this model, interactions between uranium-bearing oxidized brines derived from diagenetic processes in the sandstones and reduced fluids upwelling along faults in the basement resulted in physicochemical conditions conducive to uranium deposition. Fayek & Kyser (1997) suggested that this two-fluid model best explains the formation of the complex-type uranium deposits, and proposed a single-fluid model involving interaction between oxidizing basinal brines and basement rocks, with minimum contribution from the basement fluid, for the simple-type uranium deposits.

Samples and Analytical Methods

Approximately one thousand samples from the Athabasca basin have been investigated in this study. Most of these samples were collected as part of our previous studies of clay mineralogy in this basin (Zhang 2000, Zhang *et al*. 2001, Wasyliuk 2002). Emphasis was placed on two hundred samples from four diamond drill-holes from the Key Lake deposit (DDH2217), the McArthur River deposit (MAC223) and the BJ prospect

(MAC121 and MAC135A; Fig. 1) to document the distribution of radiation-induced damage in quartz with respect to depth, stratigraphy, structure and mineralization in the Athabasca basin. Samples from other parts of the eastern Athabasca basin also were included to document a regional distribution of radiation-induced damage in quartz and to compare results between mineralized and barren regions.

Petrographic observations and electron-microprobe analyses

All samples have been investigated in the form of polished thin sections by use of optical microscopy and back-scattered-electron (BSE) imaging on a JEOL JXA–8600 electron microprobe in order to document paragenetic relationships of quartz and associated minerals, particularly U- and Th-bearing species. Chemical compositions of U- and Th-bearing minerals in selected samples of the McArthur River deposit were determined with three automated wavelength-dispersive spectrometers on the JEOL JXA–8600 electron microprobe at the Department of Geological Sciences, University of Saskatchewan. Operating conditions for the chemical analysis of U- and Th-bearing minerals included an accelerating voltage of 20 kV, a beam current of 10 nA, beam diameters of 2 to 5 μm, counting times of 20 to 90 s, and a series of minerals, metals (*e.g.*, U, Th) and synthetic rare-earth phosphates as standards.

Cathodoluminescence imaging

Cathodoluminescence (CL) imaging was performed using a CDU CL detector on the JEOL JXA–8600 electron microprobe at the Department of Geological Sciences. Polished thin sections were first cleaned in methanol in an ultrasonic bath and then carbon-coated for CL imaging. Operating conditions for CL imaging included an accelerating voltage of 15 kV, a beam current of 50 to 150 nA, and a beam diameter of ~1 μm. Because the surface of polished thin sections may become contaminated and because CL responses degrade very quickly under high beam-currents, the electron beam was allowed to raster over the area of interest only during image acquisition. Digital CL images were acquired using the Gellar Microanalytical dPict software.

Powder X-band EPR spectroscopy

Quartz separates were obtained from twenty-four representative samples from the Key Lake and McArthur River deposits, following the method described in Part I (Botis *et al.* 2005). These separates were investigated by powder X-band (9.5–9.7 GHz) EPR with a Bruker ESP 300E spectrometer and a Bruker EMX spectrometer at the Department of Chemistry and the Saskatchewan Structural Science Centre, respectively. Efforts were made to keep all experimental conditions constant during measurements on both spectrometers, except that microwave power was varied for different experiments [from 30 dB (200 mW) to 5 dB (63.3 mW)], in order to facilitate direct comparison among the EPR spectra. In particular, all EPR spectra were collected with similar amounts of powdered materials in the same silica tube. This silica tube was shown to contain no detectable paramagnetic centers under our chosen experimental conditions. Comparisons were made only among EPR spectra recorded with the same EPR spectrometer, owing to significantly different sensitivities of the two EPR spectrometers (the Bruker EMX instrument is approximately 100 times more sensitive than the Bruker ESP 300E instrument).

Botis *et al.* (2005) showed that a comparison of EPR spectra of quartz separates before and after HF treatments allows one to determine the distribution of radiation-induced paramagnetic centers in this mineral. Accordingly, four representative samples (DDH2217–77, MAC223–635 and MAC135A–106 and –376, where DDH2217–77 denotes a sample from diamond drill-hole DDH2217 at a depth of 77 m) were selected for HF-treatment experiments. Following the method of Botis *et al.* (2005), ~100 mg quartz separates for each sample were subjected to partial dissolution with concentrated HF in sealed Teflon capsules. The HF-treated quartz separates were air-dried and then weighed to determine mass reduction. Powder X-band EPR spectra of quartz separates from these samples before and after the HF treatments were measured on the Bruker EMX EPR spectrometer at room temperature for the following microwave powers: 10, 20 and 30 dB.

RESULTS

Paragenesis and "overall" CL activity of Athabasca quartz

The Athabasca sandstones are mainly composed of quartz with variable amounts of clay and other minerals (*e.g.*, kaolinite, dickite, illite, sudoite, hematite, siderite, magnesiofoitite, crandallite–goyazite, rutile, zircon, monazite, xenotime and uraninite; Kotzer & Kyser 1995, Fayek & Kyser 1997, Zhang *et al.* 2001, Wasyliuk 2002). One characteristic feature of Athabasca quartz grains, especially those in alteration halos associated with uranium mineralization, is the common development of secondary overgrowths (Fig. 2). On the basis of petrographic evidence and data from fluid-inclusion measurements and geochemical and isotopic analyses, Kotzer & Kyser (1995; see also Fayek & Kyser 1997) distinguished two generations (Q1 and Q2) of quartz overgrowths in the Athabasca basin. Overgrowth Q1 occurs with early hematite and subsequent illite and kaolinite (and dickite; Zhang *et al.* 2001) as part of a basin-wide alteration assemblage. The Q1 overgrowths

are commonly irregular in shape (*i.e.*, variably corroded during subsequent fluid-circulation events) and are characterized by the common presence of randomly distributed inclusions of fluid and mineral particles. Q2 is present in association with magnesiofoitite (Zhang *et al*. 2001), sudoite, kaolinite and illite, and is particularly common in alteration halos around uranium deposits. The Q2 overgrowths are usually euhedral in shape and are characterized by well-developed growth-patterns defined by oscillatory or sector zoning of fluid and mineral inclusions (Kotzer & Kyser 1995). Euhedral quartz grains (up to several millimeters in size) are also common as infillings in reactivated faults, late fractures and voids.

Detrital quartz grains and their secondary overgrowths also differ markedly in their "overall" CL activity. Here, the "overall" CL activity, different from radiation-damage-induced CL described below (see also Botis *et al*. 2005), is that present throughout individual quartz grains or overgrowths, but is of uncertain origin. Detrital quartz grains are invariably more CL-active than overgrowths (Fig. 2a). Botis *et al*. (2005) reported that the CL spectra of detrital quartz grains are characterized by two broad bands in the blue (~420 nm) and red (~620–650 nm) regions, and that the CL intensities of quartz overgrowths are at least two orders of magnitude lower than those of their detrital counterparts. Similarly, several previous investigators have noted that low-temperature hydrothermal quartz is generally less CL-active than its high-temperature igneous and metamorphic counterparts (*e.g.*, Smith & Stenstrom 1965, Zinkernagel 1978).

The two generations of quartz overgrowths are also distinguishable on the basis of their "overall" CL activity. The Q1 overgrowths are either CL-inactive or exhibit weak CL with irregular patterns (Figs. 2a, b). The Q2 overgrowths commonly possess weak CL revealing oscillatory or sector zoning (Fig. 2b). Euhedral quartz grains in reactivated faults, late fractures and voids commonly exhibit weak CL revealing oscillatory or sector zoning (Fig. 2c).

Radiation-damage-induced cathodoluminescence

Botis *et al*. (2005) documented three distinct types of bright CL that are superimposed on the "overall" CL described above and are of uniform widths at ~35 to 45 μm: Type 1 as concentric halos around U- and Th-bearing mineral inclusions in quartz grains (Figs. 3a, b), Type 2 as patches along the margin of quartz grains in contact with U-bearing minerals in matrices or pores

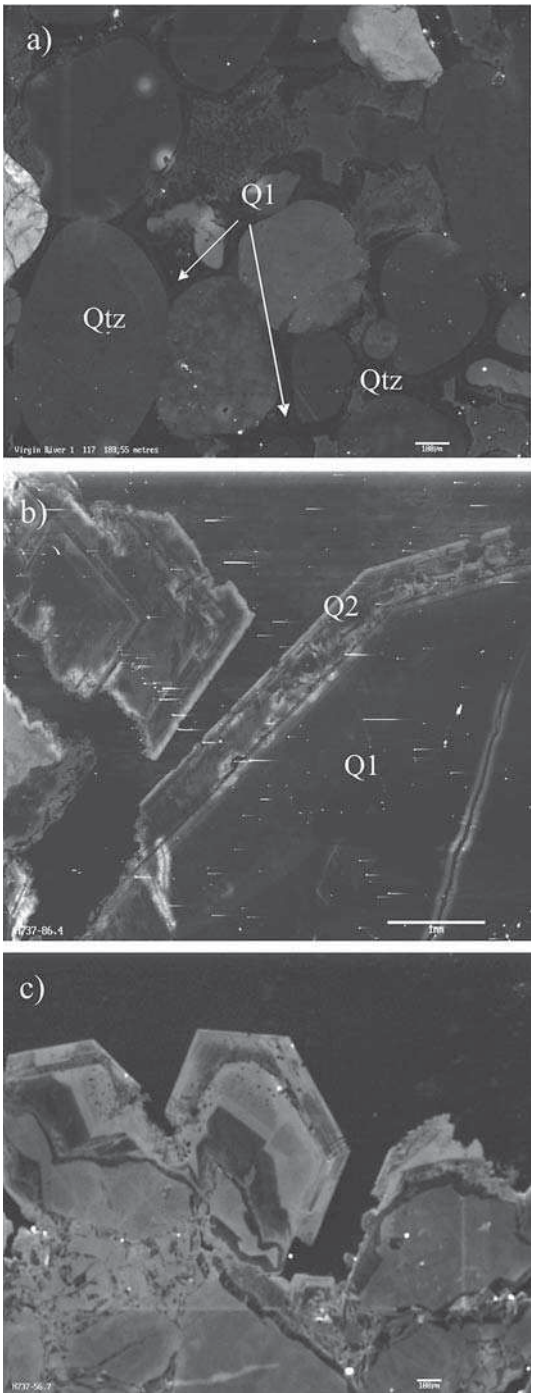

FIG. 2. Cathodoluminescence (CL) images of Athabasca sandstones illustrating: a) CL-inactive Q1 overgrowth on detrital quartz grains, b) CL-inactive homogeneous Q1 surrounded by Q2 exhibiting well-developed zoning, as revealed by weak CL, and c) euhedral quartz grains from a late fracture exhibiting oscillatory growth-zoning as revealed by CL.

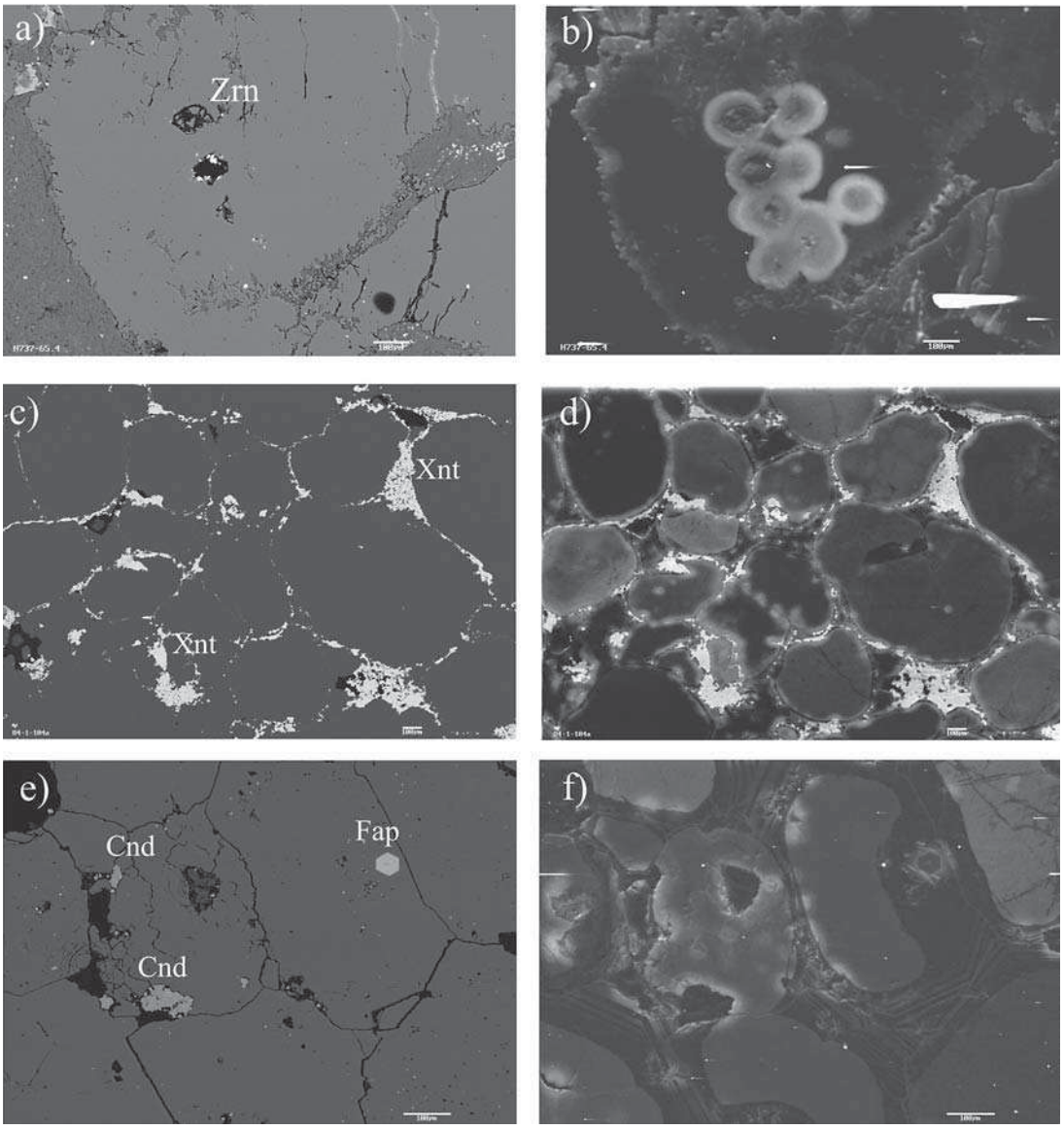

(Figs. 3c–f), and Type 3 as continuous rims on quartz grains in samples with or without any U–bearing minerals (Figs. 3g–j). Type-1 CL halos are similar to those previously reported by Owen (1988). Owen noted that the diameters of concentric CL halos around U- and Th-bearing mineral inclusions match closely the penetration distances of the most energetic alpha particles emitted from the ^{238}U, ^{235}U and ^{232}Th decay series. Owen suggested that these CL halos originate from alpha-particle-induced damage (see also Komuro *et al.* 2002). We suggest that Type-2 CL patches and Type-3 continuous CL rims, on the basis of their similar widths to Type-1 halos, are likely also caused by alpha-particle-induced damage (Meunier *et al.* 1990, Götze *et al.* 2001, Komuro *et al.* 2002, Botis *et al.* 2005). Götze *et al.* (2001) reported that the CL spectra of radiation-damage halos are characterized by a broad band at ~650 nm (see also Morton 1978, Owen 1988). Botis *et al.* (2005) noted that CL spectra of radiation-damaged areas in quartz from the Athabasca basin also have a broad band in the ultraviolet region at ~350 nm.

We have observed bright CL halos around U- and Th-bearing mineral inclusions in quartz in both sandstones and basement rocks. Such CL halos occur in both

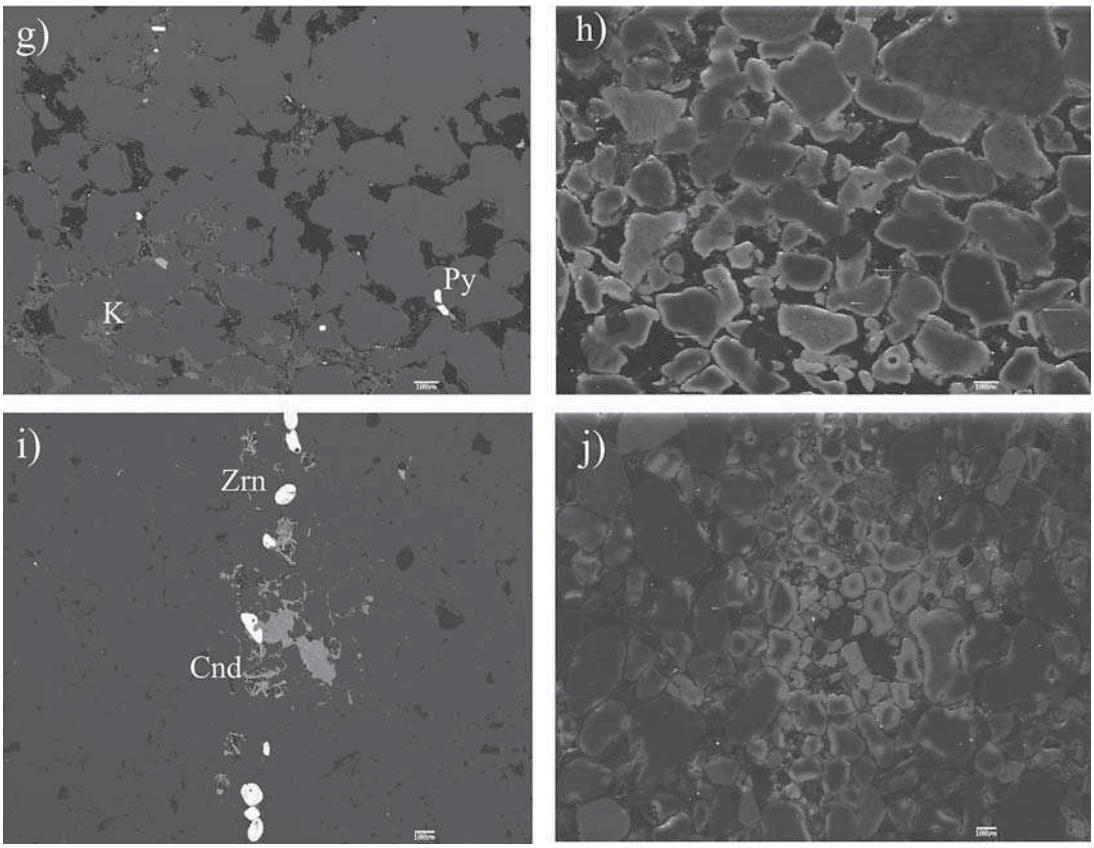

FIG. 3. Back-scattered-electron (BSE) images (a, c, e, g and i) and cathodoluminescence (CL) images (b, d, f, h and j) illustrating relationships between radiation-damage-induced CL and U-bearing minerals. a, b) Bright CL halo around zircon (Zrn) grains in detrital quartz grains from sample H737–65.4. c, d) Well-developed CL patches along the margin of detrital quartz grains in contact with massive xenotime (Xnt) in sample 84–1–104a. Note that continuous CL rims are also present on the detrital quartz grains of this sample and that CL patches on two adjacent grains of detrital quartz join together to form a complete halo. e, f) CL patches associated with crandallite (Cnd) along the boundary between detrital quartz grains and overgrowths in sample H737–58. Note the CL halo around a fluorapatite (Fap) inclusion in CL-inactive overgrowth (Q1?). g, h) Well-developed continuous CL rim on detrital quartz grains in sample MAC121–185 without any U-bearing mineral. The bright mineral is pyrite (Py), and kaolinite (K) is in the matrix. i, j) U-bearing minerals (zircon and crandallite) and continuous CL rims on quartz in a late fracture in sample MAC121–125. Note that continuous CL rims are present on quartz grains away from zircon and crandallite.

detrital quartz grains and quartz overgrowths in sandstones, and are also present occasionally in euhedral quartz grains in faults, fractures and voids. However, zircon is by far the most common U-bearing mineral inclusion in detrital quartz (Figs. 3a, b). Monazite, fluorapatite and rutile also have been found in detrital quartz, but are much less common. Crandallite and occasionally goyazite (referred to as crandallite–goyazite hereafter) are the most common U-bearing mineral inclusions in quartz overgrowths (Fig. 3e). Other U-bearing minerals in overgrowths include uraninite, xenotime (Fig. 3c), fluorapatite (Fig. 3e), monazite and rutile. U-bearing mineral inclusions in euhedral quartz grains in faults, fractures and voids, albeit rare, are similar to those observed in the overgrowths.

The CL intensity of the halos around zircon varies significantly among quartz grains, even within individual samples (Fig. 3b). Also, the CL halos associated with uraninite are notably brighter than those around other minerals (*e.g.*, crandallite–goyazite and rutile). These observations suggest correlations between CL intensity and radiation dose. However, attempts to quantify relationships between the CL intensity of halos and the U (and Th) contents in their associated mineral inclusions were not successful, presumably owing to large differences in the age of the U- and Th-bearing

minerals and difficulties in the quantification of CL intensity (see also Owen 1988).

The CL patches in contact with U-bearing minerals in matrices or pores have been observed to occur at the margins of 1) detrital quartz grains (Figs. 3d, f), 2) overgrowths (both Q1 and Q2, Fig. 3f), and 3) euhedral quartz grains in faults, fractures and voids. The suite of U-bearing minerals in matrices and pores includes crandallite–goyazite, uraninite, fluorapatite, xenotime, monazite and rutile, similar to that observed in quartz overgrowths. Similarities between CL patches and CL halos are best illustrated by those associated with U-bearing minerals along boundaries between two detrital grains or between a detrital grain and its overgrowth in mineralized sandstones, where CL patches on adjacent quartz grains or overgrowths join together to form concentric halos (Fig. 3d; see also Fig. 1a in Botis *et al*. 2005).

Continuous CL rims occur only along the margins of detrital quartz grains. They are generally uniform in intensity (Figs. 3h, j), except where they are superimposed by CL patches (Fig. 3d). Although such continuous CL rims are best developed in mineralized samples, they have been observed in samples without any visible U-bearing minerals (Fig. 3h). Even in mineralized samples, there are no direct relationships between the development of continuous CL rims and the distribution of U-bearing minerals (Figs. 3d, j). Instead, the presence of U-bearing minerals in the clay-mineral matrices usually results in the development of CL patches superimposed on a continuous CL rim (Fig. 3d). Locally, continuous CL rims have also been observed on detrital quartz grains in late fractures containing U-bearing minerals above the McArthur River deposit and its neighboring BJ prospect (Figs. 3i, j).

Distribution of radiation-damage-induced cathodoluminescence

Figure 4 illustrates the distribution of radiation-damage-induced CL in quartz from diamond drill-holes MAC135A and MAC121 at the BJ prospect (Fig. 1). The CL halos are present occasionally in quartz grains in almost all samples investigated, except for basement quartzites, in which U-bearing mineral inclusions are generally absent. Similarly, CL patches are widespread throughout the stratigraphic columns but are particularly abundant in samples containing well-developed alteration-induced assemblages, including those from 1) mineralized samples, 2) alteration halos, 3) lithological boundaries, and 4) faults, fractures and voids.

Continuous CL rims, on the other hand, are more restricted in occurrence and have been observed only in mineralized samples close to the sandstone–basement unconformity and those in alteration halos (Fig. 4). The only exception is sample MAC135A–226, which is located close to a lithological boundary but does not contain any visible U-bearing minerals. Even in the alteration halo, continuous CL rims are not developed uniformly, but are best developed in those from the siliceous cap (*i.e*., MAC135A–286; Fig. 4a) and a few other horizons (lithological boundaries) in the alteration halo (*e.g*., MAC135A–356 to 368.8; Fig. 4a). Quartz grains in sandstones from the clay-mineral-rich alteration zones usually exhibit only poorly developed CL patches associated with U-bearing minerals in the matrix, but no continuous CL rims. A well-developed continuous CL rim occurs again in the uranium-mineralized sample MAC135A–406 (Fig. 4a) and becomes more pervasive in samples toward the unconformity.

Quartz grains along an annealed microfracture of abundant crandallite–goyazite and zircon in MAC121–125 possess a continuous CL rim (Figs. 3i, j and 4b). A well-developed continuous CL rim in this hole also occurs on quartz grains from: 1) a corroded sandstone with dickite-filled pores in MAC121–185 and 2) a highly silicified sandstone with abundant uraninite and other U-bearing minerals in MAC121–275 (*i.e*., the siliceous cap; Fig. 4b). The former occurrence, where no visible U-bearing minerals are observed (Figs. 3g, h), lies directly above an aquitard where quartz overgrowths have completely removed porosity. In addition to detrital quartz grains with a well-developed continuous CL rim in sample MAC121–275, three stages of secondary quartz are observed: 1) a Q1 overgrowth with abundant U-bearing mineral inclusions, 2) a Q2 overgrowth with weak oscillatory CL, and 3) a CL-inactive euhedral quartz in cross-cutting veins. Poorly to moderately developed continuous CL rims have also been observed in sandstones close to the unconformity in MAC121 (Fig. 4b). Radiation-damage-induced CL is not observed in altered quartzites in the basement (*i.e*., MAC121–435 and –445), but CL halos associated with zircon and monazite are present in basement paragneisses (MAC121–465 and –475; Fig. 4b).

Similarly, continuous CL rims have been observed on detrital quartz grains in samples from lithological boundaries, the siliceous cap and the unconformity in MAC223 from the McArthur River deposit. Mineralized rocks in the basement close to the unconformity also exhibit well-developed continuous CL rims, and CL patches are directly associated with U-rich minerals in these samples. However, continuous CL rims and patches are conspicuously absent in altered basement rocks below the mineralized area (*e.g*., quartzite MAC223–655). Similar to those at the BJ prospect and the McArthur River deposit, CL halos around U-bearing mineral inclusions have been observed in quartz grains from all parts of the Key Lake deposit. Also, CL patches associated with U-bearing minerals in matrices and pores at the Key Lake deposit are common in mineralized samples, faults, fractures and voids. However, continuous CL rims on detrital quartz grains are rare in this deposit, except that a few samples close to the unconformity exhibit poorly to moderately developed continuous CL rims. In diamond drill-hole DDH2217,

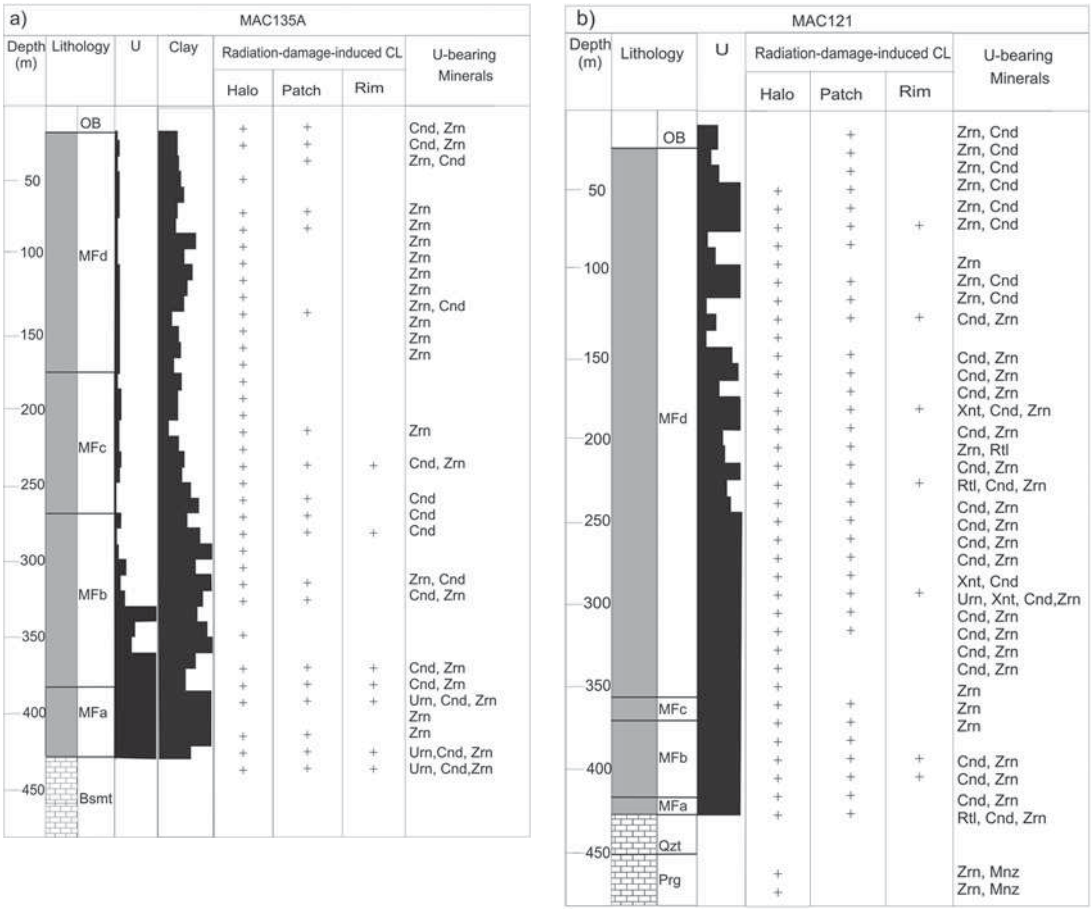

FIG. 4. Distribution of radiation-damage-induced CL (halos, patches and continuous rims) in two diamond drill-holes (a: MAC135A and b: MAC121) from the BJ prospect, near the McArthur River deposit. OB is overburden; Mfa, b, c, d are members of the Manitou Falls sandstones; Bsmt: basement rocks, Qzt: quartzite, Prg: paragneiss. Also shown for comparison are the relative abundances of total clay minerals and uranium (data provided by Cameco Corporation) and the distribution of associated U-bearing minerals (Cnd: crandallite–goyazite, Mnz: monazite; Rt: rutile, Urn: uraninite, Xnt: xenotime, Zrn: zircon).

continuous CL rims are conspicuously absent in samples DD2217–71 and –77 close to the unconformity, although CL patches are present in the former sample containing minor amounts of uraninite.

In other parts of the eastern Athabasca basin, CL halos around inclusions of U- and Th-bearing minerals are also present in detrital quartz grains in almost all sandstone samples examined in this study. Results from those samples support observations from the Key Lake and McArthur River deposits that zircon is the most common inclusion among U- and Th-bearing minerals in detrital quartz in the Athabasca basin, whereas CL halos in quartz overgrowths are mainly associated with crandallite–goyazite in sandstones and rutile in basement rocks.

Similarly, CL patches associated with U-bearing minerals in matrices and pores have been observed in altered sandstones and mineralized basement-rocks from other parts of the eastern Athabasca basin. The best-developed CL patches are again in samples close to the sandstone–basement unconformity, lithological boundaries, faults and fractures. Also, the U-bearing minerals associated with CL patches in barren regions are similar to those at the Key Lake and McArthur River deposits and include mainly crandallite–goyazite, followed by rutile, fluorapatite and xenotime.

Continuous CL rims on detrital quartz grains, on the other hand, are rare in areas away from major deposits of uranium and have been observed only locally in sandstones close to the unconformity at the Cree

Extension project and the Hughes Lake project (Fig. 1). Also, continuous CL rims from those two areas are significantly lower in intensity than those from the high-grade McArthur River deposit. It is also noteworthy that continuous CL rims have not been observed on quartz grains in annealed fractures in areas without uranium mineralization, in contrast to those at the McArthur River deposit.

Powder EPR spectra and distribution of radiation-damage-induced paramagnetic defects

The powder EPR spectra of quartz separates investigated in the present study (Fig. 5) are similar in both the number and the position of peaks to those of sample H737–58 (Botis *et al*. 2005). Our detailed EPR measurements and spectral simulations showed that the powder EPR spectra of sample H737–58 consist of at least six paramagnetic defects (Botis *et al*. 2005). The similar EPR spectra suggest that the quartz separates of this study contain the same paramagnetic defects. The relative intensity of EPR spectra of quartz separates in diamond drill-hole MAC135A (Figs. 5a, b) correlates with results from CL imaging. For example, the intensities of the EPR spectra of samples near the surface are relatively low (*e.g*., MAC135A–106 and –146; Fig. 5a). The EPR spectra of sample MAC135A–286 from the siliceous cap reveal a high concentration of radiation-induced defects (Fig. 5a). Similarly, the EPR spectra of sample MAC135A–356 close to a lithological boundary exhibit abundant radiation-induced defects (Fig. 5a). However, the EPR spectra of samples MAC135A–376 and –386 from zones of clay-mineral-rich alteration are low in intensity (Figs. 5a, b). The EPR spectra of two mineralized samples, MAC135A–406 and –416, show again abundant radiation-induced defects (Fig. 5b). These results confirm CL observations that the distribution of radiation-induced damage is not simply a function of depth, but rather is associated preferentially with the sandtone–basement unconformity, the siliceous cap and lithological boundaries (Fig. 4a).

In diamond drill-holes MAC121 and MAC223, similar distributions of radiation-induced defects are observed (Figs. 5c, d, e). In particular, well-resolved radiation-induced defects are detected in sample MAC121–385 (Fig. 5d). The EPR spectra of two basement paragneisses, MAC121–465 and –475, also reveal radiation-induced defects, but their signal-to-noise ratios are lower than that of MAC121–385 (Fig. 5d). The radiation-induced defects in these two samples are probably attributable to the presence of inclusions of U- and Th-bearing minerals (Fig. 4b). The EPR spectra of sample MAC223–225 close to a lithological boundary have well-resolved radiation-induced defects (Fig. 5e). The relatively high EPR intensity of sample MAC223–635 (Fig. 5e) is attributable to uranium mineralization in this basement sample. In basement rocks below mineralization (*e.g*., MAC223–655, an altered quartzite), however, radiation-induced defects are below the detection limit of EPR (Fig. 5e).

The EPR spectra of all samples from the Key Lake deposit are similar to those of samples from the BJ prospect and the McArthur River deposit and reveal the presence of the same radiation-induced defects (Fig. 5f). Moreover, the distribution of radiation-induced defects at the Key Lake deposit is similar to that at the McArthur River deposit. For example, the EPR spectrum with the highest intensity is obtained from a mineralized sample, DDH2217–71, close to the unconformity

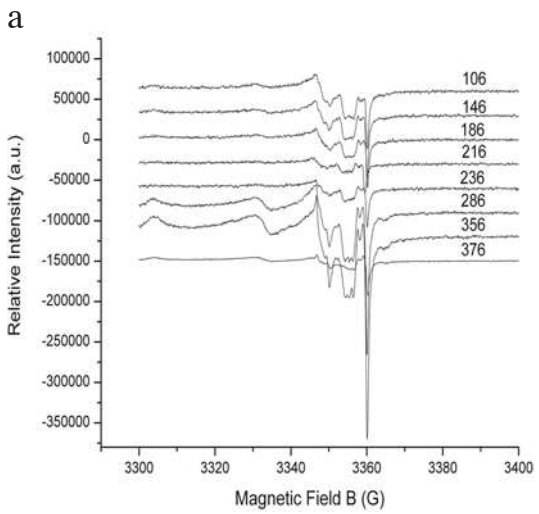

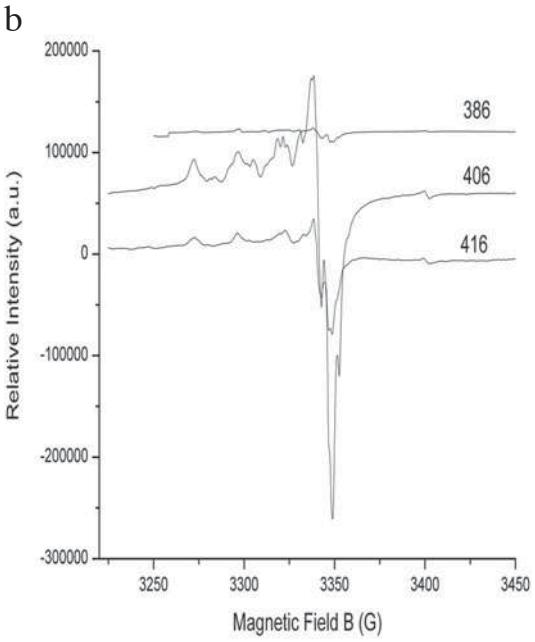

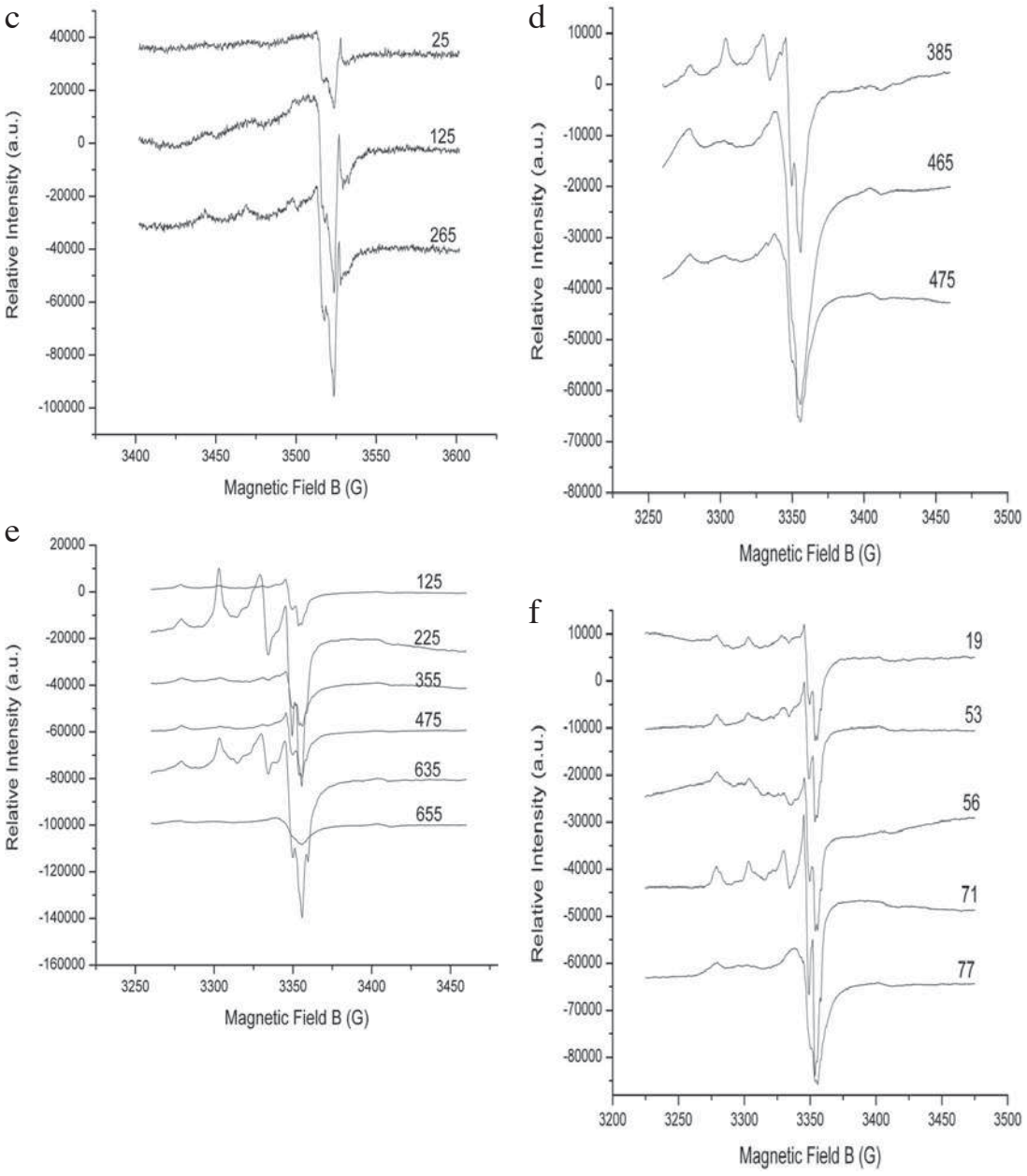

FIG. 5. Powder X-band EPR spectra of quartz separates from four diamond drill-holes: a) samples MAC135A–106 to –376 measured on the Bruker 300E spectrometer at a microwave power of 15 dB, b) samples MAC135A–386 to –416 measured on the Bruker EMX instrument at a microwave power of 15 dB; c) samples MAC121–25 to –265 measured on the Bruker 300E spectrometer at a microwave power of 5 dB; d) samples MAC121–385 to –475 measured on the Bruker EMX instrument at a microwave power of 10 dB; e) samples MAC223–125 to –655 on the Bruker EMX instrument at a microwave power of 10 dB, and f) samples DDH2217–19 to –77 measured on the Bruker EMX spectrometer at a microwave power of 10 dB.

(Fig. 5f). The EPR spectrum of sample DDH2217–77, without CL patches or continuous CL rims, also reveals the presence of radiation-induced defects (Fig. 5f).

Powder X-band EPR spectra of HF-treated quartz

In Figure 6, we compare the intensities of selected EPR peaks, representing the six paramagnetic centers identified in Part I (Botis *et al.* 2005), in four samples before and after HF treatments. Also shown for comparison are the expected EPR intensities of the six paramagnetic centers after HF treatments. Here, the expected EPR intensities are calculated from measured mass-reduction by assuming that all paramagnetic defects are evenly distributed in quartz grains. Sample MAC223–635 is an altered basement-rock containing CL patches associated with uranium mineralization. Sample MAC135A–106 is a unaltered sandstone without radiation-damage-induced CL patches or rims. Sample MAC135A–376 is an altered sandstone without radiation-damage-induced CL patches or rims from the alteration halo at the BJ prospect. Sample DDH2217–77 from close to the unconformity at the Key Lake deposit is an altered sandstone without radiation-damage-induced CL patches or rims.

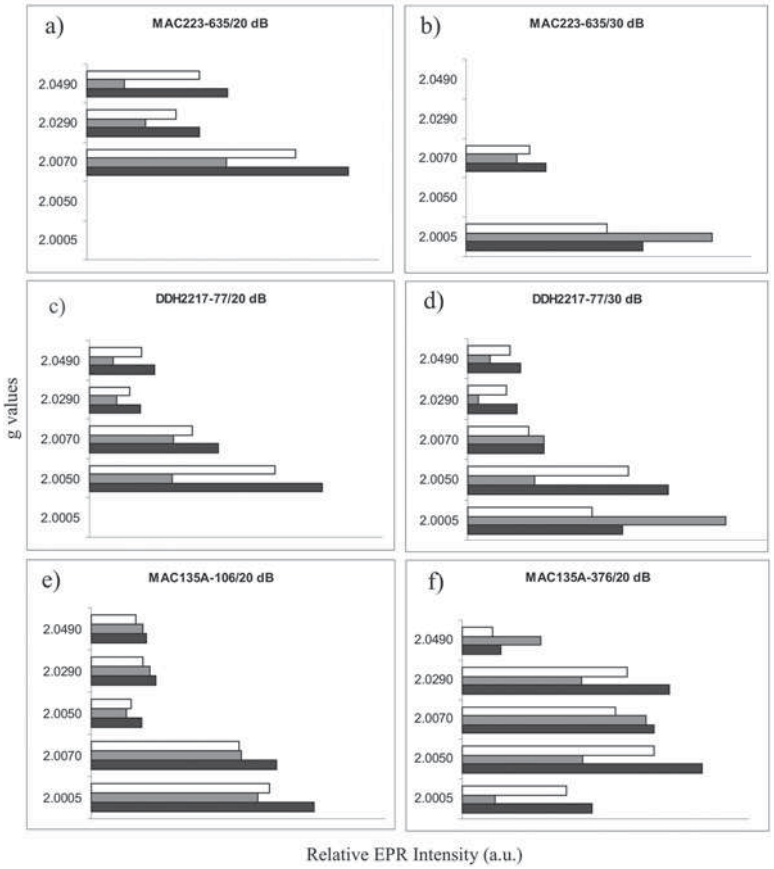

FIG. 6. Comparison of measured EPR intensities of paramagnetic centers in Athabasca quartz before (black) and after (grey) HF treatments (g = 2.0005 representing E_1'; 2.007, peroxy I and II; 2.029, O_2^{3-}/H^+(I); 2.005, O_2^{3-}/H^+(II) and 2.049, O_2^{3-}/M^+; Botis *et al.* 2005). Also shown for comparison are calculated EPR intensities of these centers on the basis of mass reduction after HF treatments (white). a, b) Sample MAC223–635 at 20 and 30 dB, respectively. c, d) Sample DDH2217–77 at 20 and 30 dB, respectively. e) Sample MAC135A–106 at 20 dB. f) Sample MAC135A–376 at 20 dB. Note that center E1' is better resolved at 30 dB, whereas the other centers are better resolved at 20 dB (see Botis *et al.* 2005 for their saturation behavior).

Similar to the results from HF-treated H737–58 described in Part I (Botis *et al*. 2005), the EPR intensities of the silicon vacancy centers and the peroxy centers in HF-treated sample MAC223–635 are significantly lower than those of their counterparts before treatments, whereas the intensity of the E_1' center (g = 2.0005) appears to increase after HF treatments (Figs. 6a, b). Botis *et al*. (2005) pointed out that this apparent "growth" of the E_1' center is attributable to removal of interferences from the other centers. It is also noteworthy that the calculated EPR intensities of the silicon vacancy centers and the peroxy centers in sample MAC223–635 are higher than the observed values after HF treatments (Figs. 6a, b). This result supports data from sample H737–58 that the silicon vacancy centers and the peroxy centers in samples with CL patches and rims are concentrated in quartz rims and fractures that are preferentially dissolved during HF treatments (Botis *et al*. 2005).

Results of sample DDH2217–77 (Figs. 6c, d) are similar to those of samples H737–58 and MAC223–635. In particular, the calculated EPR intensities of the silicon vacancy centers and the peroxy centers are notably higher than the measured values, suggesting that radiation-induced damage in quartz of this sample is also concentrated in rims and fractures. Thus, radiation-damage-induced rims and fractures, albeit not detected by CL imaging, are present in this sample.

The results of samples MAC136A–106 and –376 are similar to each other, but are different from those of samples H737–58, MAC223–635 and DDH2217–77. The measured EPR intensities of these two samples after HF treatments match closely the calculated values (Figs. 6e, f), indicating that radiation-induced damage does not occur preferentially along the rim or along fractures of quartz grains in these samples. Instead, such damage may occur in halos associated with inclusions of U- and Th-bearing minerals, which are expected to be distributed randomly in detrital quartz grains. Therefore, HF treatments do not preferentially remove the damaged areas and, thus, the EPR intensities arising from radiation-induced defects decrease in proportion to mass reduction.

Discussion

Origin of continuous CL rims on quartz

Although continuous CL rims on quartz grains are best developed in mineralized samples, they do occur in samples without any visible U-rich minerals. For example, Meunier *et al*. (1990) reported the presence of CL rims on quartz grains in sandstones from Colorado, in which uranium minerals are not present. These authors attributed such CL rims to radiation-induced damage related to uranium minerals and suggested that uranium minerals in those samples might have been leached during late hydrothermal events. However, uranium minerals, irrespective of how abundant they are, only result in CL patches at the margins of adjacent quartz grains (Figs. 3c, d) owing to the limited power of penetration of alpha particles. An alternative model is that continuous CL rims on quartz represent radiation-induced damage related to alpha particles emitted from U-bearing fluids. This model not only explains the occurrence of continuous CL rims in samples without any uranium minerals, but also can account for the uniform CL intensities in continuous rims (Fig. 3f; see also Meunier *et al*. 1990). Indeed, the occurrences of continuous rims are closely associated with the sandstone–basement unconformity, lithological boundaries and faults or fractures, all of which are characterized by well-developed alteration-induced assemblages and have been interpreted to be pathways of uranium-bearing mineralizing fluids. Similarly, the local occurrence of continuous CL rims on quartz grains in fractures above the McArthur River deposit and the BJ prospect (Fig. 3j) can be attributed to late uranium-bearing fluids (see below).

Comparison of CL imaging and EPR spectroscopy

In this study, we show that both CL imaging and EPR spectroscopy are capable of detecting natural radiation-induced damage in quartz. With *in situ* CL imaging, we are able to distinguish three types of radiation-induced damage (*i.e*., halos, patches and continuous rims), which allow the documentation of their paragenetic relationships with respect to host quartz grains and other associated minerals, including U-bearing minerals (Figs. 2, 3). Powder EPR spectroscopy is a bulk technique requiring time-consuming separation of minerals, but it allows us to identify specific paramagnetic defects that cause the characteristic CL (Botis *et al*. 2005). A major advantage of EPR spectroscopy over CL imaging (and optical techniques in general) is its superior sensitivity in detecting and characterizing low levels of paramagnetic defects (see also Pan *et al*. 2002, and references therein). This superior sensitivity is demonstrated by the presence of radiation-damaged rims and fractures in quartz from sample DDH2217–77, which were revealed by EPR but were not detected by CL imaging. Similarly, EPR spectra show that radiation-induced defects are present in "unaltered" sandstones, in which CL patches or rims are not observed. Therefore, CL imaging and EPR spectroscopy are complementary techniques in characterizing natural radiation-induced damage in quartz.

Implications for uranium mineralization

With CL imaging, it is possible to readily distinguish detrital quartz grains from the less-intensive CL overgrowths (see also Smith & Stenstrom 1965, Zinkernagel 1978). Also, the two generations of secondary overgrowths on quartz have distinct CL activity. Therefore,

CL imaging is a useful tool for establishing paragenesis of quartz in Athabasca sandstones. A notable feature of the radiation-damage-induced CL is its high annealing temperature (*i.e.,* stable after annealing up to 800°C, Baker & Owen 1983, Owen 1988, Botis *et al.* 2005). Therefore, radiation-damage-induced CL is potentially applicable to paragenetic studies of quartz from metamorphosed sedimentary basins.

If our interpretation of continuous CL rims on quartz to record bombardments of alpha particles from U-bearing fluids is correct, this type of radiation-damage-induced CL provides a new visual method for mapping the pathways of mineralization fluids in the Athabasca basin and elsewhere. Indeed, the restricted distribution of continuous CL rims at the McArthur River deposit suggests that they are an excellent indicator of uranium mineralization, hence potentially useful in exploration for new uranium deposits. However, the general lack of continuous CL rims on quartz grains in samples close to the unconformity at the Key Lake deposit and other parts of the Athabasca basin suggests that with CL imaging, it is not possible to detect weak radiation-induced damage. We caution, therefore, that an absence of the characteristic CL rims on quartz grains from sedimentary basins cannot be taken as evidence to rule out uranium mineralization.

In contrast to well-developed radiation-induced damage in most Athabasca sandstones and mineralized basement rocks, radiation-induced damage is conspicuously absent in quartz grains from altered basement-rocks below the mineralized area at the McArthur River deposit (*e.g.*, MAC223–655). Similarly, radiation-induced damage (except for that associated with inclusions of U- and Th-bearing minerals) in quartz grains in altered basement-rocks below the mineralized area at the Key Lake deposit and the BJ prospect is below the detection limit of the EPR technique. These altered basement-rocks were collected from fault zones that have been interpreted to be the conduits for basement fluids during the formation of uranium deposits. This absence of radiation-induced damage in quartz grains from those altered basement-rocks suggests that basement fluids were poor in uranium, supporting previous genetic models that mineralization in the Athabasca basin resulted from either interactions of U-rich basinal fluids and U-poor basement fluids in the formation of the complex-type uranium deposits or interactions between basinal fluids and basement rocks in the formation of the simple-type deposits (Hoeve & Quirt 1984, Kotzer & Kyser 1995, Fayek & Kyser 1997).

The occurrence of continuous CL rims on detrital quartz grains is at least partly attributable to structural differences between detrital quartz and overgrowths. The detrital grains, of mostly high-temperature igneous or metamorphic origin, are expected to contain more abundant intrinsic defects (*i.e.*, silicon and oxygen vacancies, substitutional and interstitial ions, *etc.*) than the overgrowths, of low-temperature hydrothermal formation (~200°C; Kotzer & Kyser 1995). Nevertheless, the occurrences of continuous CL rims on detrital quartz grains (Figs. 3d, h) suggest that uranium was present in early diagenetic fluids. This suggestion is supported by the common occurrence of U-bearing minerals along boundaries between detrital quartz grains and Q1 overgrowths (Fig. 3e), which also indicates uranium deposition during an early diagenetic event. Therefore, uranium mineralization in the Athabasca basin could have begun earlier than most authors have postulated; they favored the main event of mineralization during the peak diagenesis after early silicification (Kotzer & Kyser 1995, Fayek & Kyser 1997, Fayek *et al.* 2002). We agree that the main stage of mineralization occurred after the formation of the regional Q1 overgrowths, but emphasize the local abundance of U-bearing minerals, including uraninite, in both Q1 and Q2 overgrowths. The presence of continuous CL rims on quartz grains along annealed fractures in overlying sandstones at the McArthur River deposit and the BJ prospect provides direct evidence for late remobilization of uranium (*cf.* Kotzer & Kyser 1995, Fayek & Kyser 1997, Fayek *et al.* 2002). This late remobilization also is supported by the common occurrence of CL patches around U-bearing minerals in reactivated faults, late fractures and voids.

Halos of hydrothermal alteration surrounding individual orebodies in the Athabasca basin have been proposed to be an integral part of the processes of uranium mineralization (Hoeve & Quirt 1984, Kotzer & Kyser 1995, Fayek & Kyser 1997, Zhang *et al.* 2001). Radiation-induced damage in quartz would be expected in sandstones throughout those alteration halos. At the McArthur River deposit and the BJ prospect, however, radiation-induced damage in quartz is generally absent in sandstones from the clay-mineral-rich zones of alteration between the siliceous cap and the unconformity (Figs. 4, 5). One possible explanation is that U-bearing mineralizing fluids in those two areas were highly channeled (*i.e.*, along the unconformity, lithological boundaries and the siliceous cap). Alternatively, radiation-induced damage in quartz from clay-mineral-rich zones of alteration may have been removed during hydrothermal alteration because detrital quartz grains in those zones are characterized by high degrees of corrosion and, locally, complete dissolution.

Acknowledgements

We thank Grant S. Henderson, Roger A. Mason and Robert F. Martin for incisive criticism and helpful suggestions, David Thomas and Kenneth Wasyliuk of the Cameco Corporation for their continuing support and assistance, and the Cameco Corporation and NSERC for financial support.

REFERENCES

ARMSTRONG, R.L. & RAMAEKERS, P. (1985): Sr isotopic study of Helikian sediment and diabase dikes in the Athabasca basin, northern Saskatchewan. *Can. J. Earth Sci.* **22**, 399-407.

BAKER, E.B. & OWEN, M.R. (1983): 800°C threshold for cathodoluminescence in zircon and radiation-damage haloes in metaquartzite. *Geol. Soc. Am., Abstr. Programs* **18**, 532.

BOTIS, S., NOKHRIN, S.M., PAN, YUANMING, XU, YINGKAI, BONLI, T. & SOPUCK, V. (2004): Radiation-damage-induced cathodoluminescence in quartz: an EPR and micro-Raman study. *Geol. Assoc. Can. – Mineral. Assoc. Can., Program Abstr.* **29**, 69.

BOTIS, S., NOKHRIN, S.M., PAN, YUANMING, XU, YINGKAI, BONLI, T. & SOPUCK, V. (2005): Natural radiation-induced damage in quartz. I. Correlations between cathodoluminescence colors and paramagnetic defects. *Can. Mineral.* **43**, 1565-1580.

CUMMING, G.I. & KRSTIC, D. (1992): The age of unconformity-related uranium mineralization in the Athabasca Basin, northern Saskatchewan. *Can. J. Earth Sci.* **29**, 1623-1639.

FAYEK, M. & KYSER, T.K. (1997): Characterization of multiple fluid-flow events and rare-earth element mobility associated with formation of unconformity-type uranium deposits in the Athabasca basin, Saskatchewan. *Can. Mineral.* **35**, 627-658.

FAYEK, M., KYSER, T.K. & RICIPUTI, L.R. (2002): U and Pb isotope analysis of uranium minerals by ion microprobe and the geochronology of the McArthur River and Sue zone uranium deposits, Saskatchewan, Canada. *Can. Mineral.* **40**, 1553-1569.

HOEVE, J. & QUIRT, D. (1984): Mineralization and host rock alteration in relation to clay mineral diagenesis and evolution of the Middle-Proterozoic Athabasca Basin, northern Saskatchewan. *Sask. Res. Council, Tech. Rep.* **157**.

HOEVE, J. & SIBBALD, T.I.I. (1978): On the genesis of Rabbit Lake and other unconformity-type uranium deposits in northern Saskatchewan, Canada. *Econ. Geol.* **73**, 1450-1473.

GÖTZE, J., PLÖTZE, M. & HABERMANN, D. (2001): Origin, spectral characteristics and practical applications of the cathodoluminescence (CL) of quartz: a review. *Mineral. Petrol.* **71**, 225-250.

KOMURO, K., HORIKAWA, Y. & TOYADA, S. (2002): Development of radiation-damage halos in low-quartz: cathodoluminescence measurement after He^+ ion implantation. *Mineral. Petrol.* **76**, 261-266.

KOMURO, K., YAMAMOTO, M., FUJIKI, S., FUKUSHIMA, T. & KOYAMA, K. (1995): Development of radiation-damage rims in quartz around the Kanyemba–1 uranium deposit, Zimbabwe. *Annu. Rep. Inst. Geosci. Univ. Tsukuba* **21**, 65-69.

KOTZER, T.G. & KYSER, T.K. (1995): Petrogenesis of the Proterozoic Athabasca Basin, northern Saskatchewan, Canada, and its relation to diagenesis, hydrothermal uranium mineralization and paleohydrology. *Chem. Geol.* **120**, 45-89.

KOTZER, T.G., KYSER, T.K. & IRVINE, E. (1992): Paleomagnetism and evolution of fluids in the Proterozoic Athabasca Basin, northern Saskatchewan, Canada. *Can. J. Earth Sci.* **29**, 1474-1491.

KYSER, T.K., HIATT, E., RENAC, C., DUROCHER, K., HOLK, G.& DECKERT, K. (2000): Diagenetic fluids in Paleo- and Meso-Proterozoic sedimentary basins and their implications for long protracted fluid histories. *In* Fluids and Basin Evolution (T.K. Kyser, ed.). *Mineral. Assoc. Can., Short-Course Vol.* **28**, 225-262.

MARSHALL, D.J. (1988): *Cathodoluminescence of Geological Materials*. Unwin Hyman, Boston, Massachusetts.

MEUNIER, J.D., SELLIER, E. & PAGEL, M. (1990): Radiation-damage rims in quartz from uranium-bearing sandstones. *J. Sed. Petrol.* **60**, 53-58.

MORTON, R.D. (1978): Cathodoluminescence applied to uranium exploration. *Nucl. Spectrosc.* **11**, 1.

OWEN, M.R. (1988): Radiation-damage haloes in quartz. *Geology* **16**, 529-532.

PAN, YUANMING, FLEET, M.E., CHEN, NING, WEIL, J.A. & NILGES, M.J. (2002): Site preference of Gd in synthetic fluorapatite by single-crystal W-band EPR and X-ray refinement of the structure: a comparative study. *Can. Mineral.* **40**, 1103-1112.

PERCIVAL, J.B., BELL, K. & TORRANCE, J.K. (1993): Clay mineralogy and isotope geochemistry of the alteration halo of the Cigar Lake uranium deposit (Canada). *Can. J. Earth Sci.* **30**, 689-704.

SMITH, J.V. & STENSTROM, R.C. (1965): Electron-excited luminescence as a petrologic tool. *J. Geol.* **73**, 627-635.

WASYLIUK, K. (2002): *Petrogenesis of the Kaolinite-Group in the Eastern Athabasca Basin of Northern Saskatchewan: Applications to the Uranium Mineralization*. M.Sc.thesis, Univ. Saskatchewan, Saskatoon, Saskatchewan.

ZHANG, AIMIN, PAN, YUANMING, SOPUCK, V., UPADRASHTA, Y. & WEIL, J.A. (2002): Cathodoluminescence colors in quartz and possible relationships to structural defects. *Geol. Assoc. Can. – Mineral. Assoc. Can., Program Abstr.* **27**, 131.

ZHANG, GUANGYU (2000): *Characterization of Clay Minerals in the Athabasca Basin Using Shortwave Infrared (SWIR) Reflectance Spectroscopy*. M.Sc. thesis, Univ. Saskatchewan, Saskatoon, Saskatchewan.

ZHANG, GUANGYU, WASYLIUK, K. & PAN, YUANMING (2001): The characterization and quantitative analysis of clay minerals in the Athabasca basin, Saskatchewan: application of shortwave infrared reflectance spectroscopy. *Can. Mineral.* **39**, 1347-1363.

ZINKERNAGEL, U. (1978): Cathodoluminescence of quartz and application to sandstone petrology. *Contrib. Sed.* **8**, 1-69.

Received August 31, 2005, revised manuscript accepted August 31, 2006.